SEMINÁRIOS PPG-EM / UERJ 2020

PPG-EM UERJ 2020 SEMINARS

Programa de Pós-graduação em Engenharia Mecânica UERJ

Graduate Program in Mechanical Engineering UERJ

SEMINÁRIOS PPG-EM / UERJ 2020

PPG-EM UERJ 2020 SEMINARS

Programa de Pós-graduação em Engenharia Mecânica UERJ

Graduate Program in Mechanical Engineering UERJ

WWW.PPGEM.UERJ.BR

Editado por Prof. Daniel J. N. M. Chalhub.

Capa: *"Rover em Marte - Conceito artístico"*. Créditos de imagem: Usuário Wilkilmages do Pixbay. https://pixabay.com/photos/mars-mars-rover-space-travel-rover-67522/

Foto dos cabeçalhos:*"Marte - Paisagem do planeta vermelho"*. Créditos de imagem: Usuário Wilkilmages do Pixbay. https://pixabay.com/photos/mars-planet-red-planet-surface-11656/

Edited by Prof. Daniel J. N. M. Chalhub.

Cover: *"Mars rover - Concept art"*. Image by Pixabay user Wilkilmages https://pixabay.com/photos/mars-mars-rover-space-travel-rover-67522/

Header image: *"Mars - Red planet landscape"*. Image by Pixabay user Wilkilmages https://pixabay.com/photos/mars-planet-red-planet-surface-11656/

April 06, 2021

Sumário / Contents

1. Mini-artigos / Short papers

06 de abril de 2021

Neste capítulo são apresentados os mini-artigos dos doze trabalhos científicos que fizeram parte dos Seminários do PPG-EM em 2020. Devido a pandemia de COVID-19, os Seminários do PPG-EM 2020 foram realizados em formato online. Os trabalhos estão organizados segundo a data de apresentação.

Prof. Daniel J. N. M. Chalhub, D.Sc.
Coordenador dos Seminários PPG-EM 2020

April 06, 2021

This chapter presents the short papers of the twelve scientific works that participated in the PPG-EM Seminars in 2020. Due to the COVID-19 pandemic, the PPG-EM 2020 Seminars were held online. Papers are organized according to the date of presentation.

Prof. Daniel J. N. M. Chalhub, D.Sc.
PPG-EM 2020 Seminars Chair

PERFORMANCE ANALYSIS OF A FRACTIONAL CONTROL IN A NONLINEAR INVERTED CART-PENDULUM SYSTEM

Author: Julio Cesar Basilio[1] *basilio.julio@posgraduacao.uerj.br*
Advisor(s): Americo Cunha Jr[1] ; José Geraldo Telles[1]
[1] Rio de Janeiro State University

August 05, 2020
PPG-EM Seminars: season **2020**
http://www.ppgem.uerj.br

Keywords: fractional calculus, state feedback, fractional-order control, cart-pendulum system.

1 Introduction

The use of fractional-order controllers to drive dynamic systems to a desired configuration has become popular in the past decade, with many studies claiming that they perform better when compared to integer-order equivalents, especially for non-linear systems.

The idea of fractional calculus was introduced in 1695 with Bernoulli, Leibniz and L'Hôpital [5]. In the following centuries, many pure and applied mathematicians contributed to the development of the theory of fractional calculus, including the fractional derivatives of Grünwald-Letnikov and Riemann-Liouville (Eq. 1) [3]. The development of new definitions is an active field of research in mathematics [1] , but in the last decade, mainly thanks to the development of numerical methods to simulate fractional systems [7], fractional operators began to be used in engineering analysis [2] and control theory [6]. Among the favorable characteristics that these fractional operators offer, highlighted the fractional exponent offers a type of additional degree of freedom to adjust a controller, opening opportunities for performance improvements in the controller design.

$$\mathcal{I}^{\alpha} f(t) = \frac{1}{\Gamma(\alpha)} \int_0^t (t-\tau)^{\alpha-1} f(\tau)\, d\tau \qquad (1)$$

Exploring the second characteristic, this work aims to analyze the performance of a controller using fractional-order integrators and compare them to the integer-order. This analysis is performed in a state-feedback control system proposed to stabilize an inverted cart-pendulum system (Fig. 1), chosen as a reference because it is a nonlinear system widely studied using integer-order controllers, which also began to be tested in the fractional control literature [4].

2 Methodology

The system dynamics evolves according to the following nonlinear model

$$\begin{aligned} (J + m\,l^2)\,\ddot{\theta} - m\,g\,l\,\sin\theta &= -m\,l\,\ddot{x}\,\cos\theta \\ (m+M)\,\ddot{x} + m\,l\,\ddot{\theta}\,\cos\theta - m\,l\,\dot{\theta}^2\,\sin\theta &= u\,, \end{aligned} \qquad (2)$$

where θ is the angular position and x is car position.

The control system is implemented and executed in Simulink, according to the schematic of the controller diagram shown in Fig. 1, where r is the reference input signal; e is the tracking error; u is the control signal; K_1, K_2, K_3, K_4, K_l are the control gains; $\mathcal{I}^{\alpha_1}$, $\mathcal{I}^{\alpha_2}$, $\mathcal{I}^{\alpha_3}$, $\mathcal{I}^{\alpha_l}$ are the integrators, if $\alpha \in \mathbb{Z}$ (integer-order) and if $\alpha \notin \mathbb{Z}$ (fractional order).

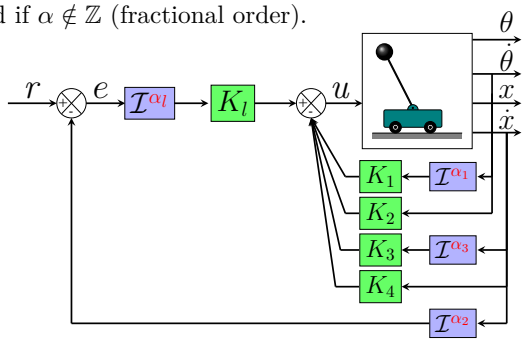

Figure 1: Schematic illustration of the proposed controller for the inverted cart-pendulum system

The strategy is to employ the linear Pole Placement method to calculate the controller gains and then compare the performance between integer-order integrators and different fractional-order combinations, the latter calculated using an optimization method based on in the performance index chosen to minimize. The controller performance indices used were: integrated square error $ISE = \int_0^t e(t)^2 dt$; settling time (ST) and integrated square control signal $ISU = \int_0^t u(t)^2 dt$. The first two indices related to θ and x. The latter index quantify the control effort. The performance of the system is obtained changing the orders of the integrators by simulations using the FOMCOM toolbox [7], considering the initial conditions: $\theta_0 = 10^o$; $\dot{\theta} = 0$; $x_0 = 0$; $\dot{x}_0 = 0$.

3 Results

The results of the simulations shown in Fig. 2, where the darker regions indicate the lowest values, already show that fractional-order integrators improve the system. However, there are different combinations of orders for each index evaluated. Based on this, four optimizations are performed to minimize each of the performance indices, with restrictions that all indices are lower than the performance of the controller using integer-order and ISU at most 25% higher.

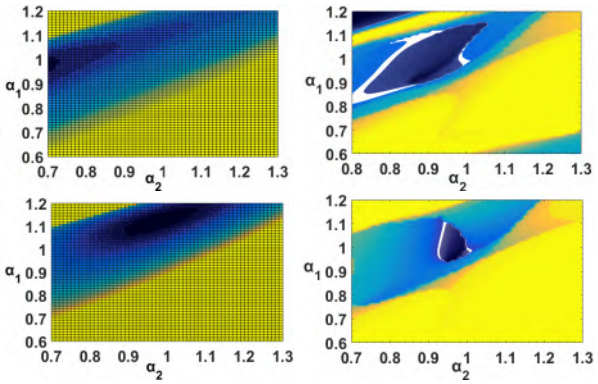

Figure 2: Simulation results with different α_1 and α_2 for performance indices: ISE_θ (left top) and ST_θ (right top) angular position; ISE_x (left bottom) and ST_x (right bottom)

The orders of the integrators and their performance resulting from the optimizations, shown in Table 1, show the improving the controller in all analyzed indices, as in the case of the optimization of ST_θ, with 30% improvement, while the other indices change little. Another case is the optimization of ISE_x, with 14% improvement, and the other indices have also improved, as shown in Fig. 3, with the comparison of the dynamic responses of the integer-order and the fractional-order.

Table 1: Optimization results with optimal orders integrators and their performance values.

$ISE_{\theta min}$	$ISE_{x min}$
$\alpha_1 = 1.08$ / $\alpha_2 = 0.94$	$\alpha_1 = 1.09$ / $\alpha_2 = 0.95$
$ISE_\theta = 0.016$ (-23%) $ISE_x = 0.22$ (-13%) $ST_\theta = 4.22$ (-13%) $ST_x = 5.02$ (- 1%)	$ISE_\theta = 0.016$ (-23%) $ISE_x = 0.22$ (-14%) $ST_\theta = 4.19$ (-14%) $ST_x = 4.91$ (- 3%)

$ST_{\theta min}$	$ST_{x min}$
$\alpha_1 = 0.96$ / $\alpha_2 = 0.93$	$\alpha_1 = 1.00$ / $\alpha_2 = 0.99$
$ISE_\theta = 0.021$ (- 1%) $ISE_x = 0.26$ (-0.3%) $ST_\theta = 3.40$ (-30%) $ST_x = 4.99$ (- 2%)	$ISE_\theta = 0.020$ (- 3%) $ISE_x = 0.25$ (- 2%) $ST_\theta = 4.84$ (- 1%) $ST_x = 3.97$ (-22%)

A study of the basin of attraction of the initial angular position and the initial angular velocity was also carried out, showing a reduction of the basin for the optimal orders ($\alpha_1 = 1.09$ and $\alpha_2 = 0.95$) compared to the integer-order controller. However, a combination of fractional-orders was found that increased the basin of attraction, as shown in Fig. 4.

4 Discussion and Conclusion

These results show that the fractional-order controller achieved a better response.

- improved transient;
- error reduction;
- possibility of improving performance without increasing control effort;
- for some specific cases, larger attraction domains;

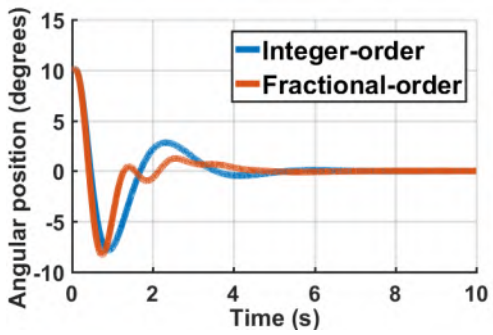

Figure 3: Time series of the angular position with integer and fractional-order integrators.

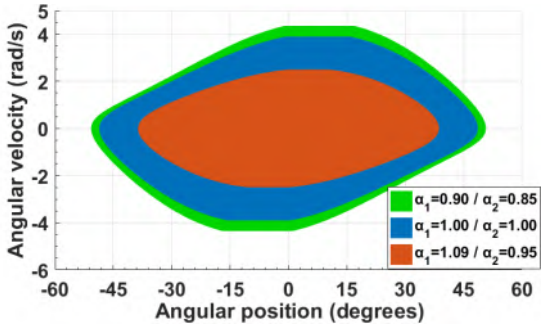

Figure 4: Basins of attraction in the angular position vs angular velocity plane for the three cases of the integrators.

References

[1] Mauro CAPUTO, Michele; FABRIZIO. A new definition of fractional derivative without singular kernel. *Progress in Fractional Differentiation and Applications*, 1, 2015.

[2] John T. KATSIKADELIS. Generalized fractional derivatives and their applications to mechanical systems. *Archive of Applied Mechanics*, 85, n.9-10: 1307–1320, 2015.

[3] C. Li and W. Deng. Remarks on fractional derivatives. *Applied Mathematics and Computation*, 187: 777–784, 2007.

[4] Mohamed A.; HASSAN MA Moustafa MOUSA, M. E.; EBRAHIM. Optimal fractional-order proportional—integral—differential controller for inverted pendulum with reduced order linear quadratic regulator. In *Fractional-order Control and Synchronization of Chaotic Systems*, Cham, 2017.

[5] JA Tenreiro ORTIGUEIRA, Manuel D.; MACHADO. What is a fractional derivative? *Journal of computational Physics*, 293:4–13, 2015.

[6] Aleksei TEPLJAKOV. *Fractional-order modeling and control of dynamic systems*. Springer, 2017.

[7] Eduard; BELIKOV Juri TEPLJAKOV, Aleksei; PETLENKOV. Fomcom: a matlab toolbox for fractional-order system identification and control. *International Journal of Microelectronics and computer science*, 2, n.2:51–62, 2011.

LOW COST SOLAR COLLECTORS: CONSTRUCTION PROPOSALS, TECHNICAL AND ECONOMIC VIABILITY.

Author: Thiago Queiroz Alvares[1] *thiagoqa2@gmail.com*
Advisor(s): Manoel Antonio da Fonseca Costa Filho[1]
[1] Rio de Janeiro State University

August 05, 2020
PPG-EM Seminars: season **2020**
http://www.ppgem.uerj.br

Keywords: Solar collectors, low cost, solar radiation.

1 Introduction

Brazil has a privileged solar potential available, with an average daily irradiation between 3500 to 5500 W.h / m2.day. In addition, according to [2] the greatest use of the electric shower occurs precisely at peak hours, between 18:00 and 21:00 hours, which leads to a greater overload of the Generation, Transmission and Distribution systems and higher spending by households. Therefore, solar heating is configured as an alternative to domestic water heating, running integrally or complementary way to electric energy, in addition to being a sustainable source. However, the greater acceptance of solar heating finds the following limiting factors: the high value of solar heaters present in the market, the difficulty in accessing technical assistance or spare parts in several regions of Brazil and the absence of mixers in showers in low-income homes. The intention of the present work is to present the feasibility of models of solar collectors that combine reduced value and a scale production.

2 Materials and Methods

To develop the configuration of the proposed collectors, the geometry and materials that would be used were initially defined. Afterwards, the costs of construction materials were defined. Then, the literature equations for the proposed configurations were developed, with the calculation of the following parameters using the Engineering Equation Solver (EES) software: thermal efficiency of the collector, thermal efficiency of the entire system (collector plus reservoir) for each configuration. The data found were validated using the Transient System Simulation Tool (TRNSYS) software.

2.1 Configurations

The first configuration uses a honeycomb polycarbonate plate as a solar collector and the second, uses a roof tile and an aluminum plate. The polycarbonate collector has an absorbing plate with a 6 mm honeycomb polycarbonate plate through which water circulates, inserted in a naval plywood box, with rock wool as a thermal insulator and, sealing the box, a cover of 4 mm thick glass.

In the second configuration, the absorber plate consists of a flat aluminum plate joined by weld seam to an aluminum tile, thus creating channels through which water can circulate. The set is also inserted in a naval plywood box, with rock wool as a thermal insulator among them. A 4 mm thick glass plate seals this box. Both absorber plates are painted with a special matte black paint to improve the absorption of incident solar radiation. The hot water reservoir in both configurations consists of the use of a 200 L polyethylene drum sold commercially, inserted in another fiberglass drum, built for this purpose. This other drum must have dimensions such that, between its internal walls and the external walls of the polyethylene drum, there is a gap of approximately 5 cm. Rock wool is also placed in this gap for thermal insulation. The interconnection between the collector and the reservoir is carried out by thermally insulated PVC pipes.

2.2 Thermal Modeling of Collectors

For thermal modeling of the collectors, the model proposed by [1] was used, adapting to the geometries of the proposed collectors. In this model, after calculating the solar radiation that the collector receives, its thermal losses are calculated. Considering the thermal resistance model, the losses are divided as follows: top losses, losses at the sides and losses at the rear of the collector. Figure 1 presents this analogy.

With the irradiation value that the collector receives and its losses, it is possible to calculate the thermal efficiency. For the determination of solar irradiation, the region of the Campo Grande neighborhood in Rio de Janeiro was considered because this region has an abundant number of houses. The irradiation data were obtained from the website of the National Institute for Space Research (INPE).

3 Results

Research on the values of commercial flat solar collectors was carried out. The average sale value is 175.55 dollars and the average sale value of commercial models with their respective storage tanks is 498.16 dollars.

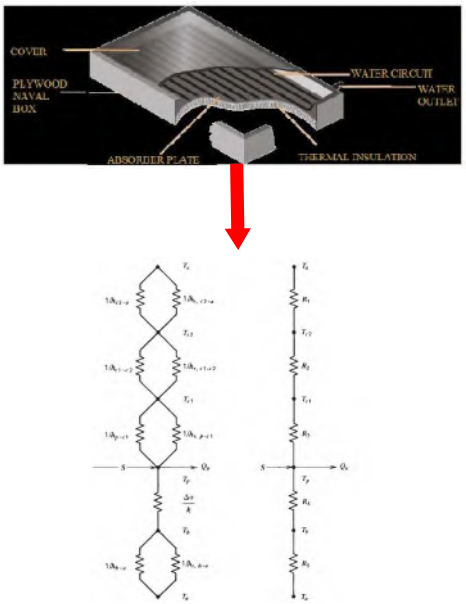

Figure 1: Model of thermal resistance of the flat solar collector.

Considering the national minimum wage in August 2020 of 197.19 dollars, the average selling price of the collector represents 88.99 percent of the minimum wage and, for the kit of the collector with the tank, it represents 252.63 percent.

For configuration I, the estimated price of the collector's building materials is 21.36 dollars and the estimated price of the building materials for the collector and tank assembly is 198.13 dollars. These values represent 52.42 percent and 100.48 percent of the minimum wage, respectively. For configuration II, the estimated price of the collector's building materials is 160.39 dollars and the estimated price of the building materials for the collector and tank assembly is 245.31 dollars. These values represent 52.42 percent and 100.48 percent of the minimum wage, respectively.

With regard to thermal performance, initial calculations indicate that the thermal performance of the system, although lower than that of commercial collectors, approaches their values.

4 Conclusions

After defining the geometry of the solar collectors and carrying out their thermal modeling, it is possible to conclude that:

- The cost is lower than that of commercial collectors;
- It is feasible to build collectors at scale;
- Initial calculations indicate that the thermal performance of the system, although lower than that of commercial collectors, approaches the values of these;
- For future work, it is suggested to assemble and test the best efficiency prototype.

References

[1] John A. Duffie. *Solar Engineering of Thermal Processes*. John Wiley ans Sons, 2013.

[2] Enio Bueno Pereira et al. Atlas brasileiro de energia solar. Technical report, INPE, 2017.

PPG-EM
Programa de Pós-graduação em Engenharia Mecânica

ELECTRIC VEHICLE CHARGING DIVERSITY FACTOR

Author: Windson Braga Pereira[1] *windsonbraga@hotmail.com*
Advisor(s): Luiz Artur Pecorelli Peres[1]
[1] Rio de Janeiro State University

August 05, 2020
PPG-EM Seminars: season **2020**
http://www.ppgem.uerj.br

Keywords: Electric vehicles charging, smart city, diversity factors.

1 Introduction

This short paper compares the deterministic and stochastic approach to determine the increase in demand on the transformer load curve due to the recharging of electric vehicles (EVs) and the diversity factors associate. Initially, it's presented the behavior of EVs charging demand from tests performed [5, 6, 4] and after, their treatment to represent the average power accounted for at discrete 15-minute time intervals corresponding to the standards used by the electricity companies in Brazil. The method is applicable for the analysis of transformer capacity and can also be extended to medium voltage feeders of networks. The vehicle provided by ENEL for charging tests was the Palio Weekend Electric powered by ZEBRA battery [2, 7] and assembled by Itaipu Binacional through a technology cooperation agreement with KWO of Switzerland in partnership with Fiat of the Brazil [1]. From these procedures, the simulation model considers the effect of random variables related to the distance previously traveled [3] by the vehicle and their connection instant to the electric network.

2 EV's active power curve

"Figure (1)" illustrates the graphs of typical active and reactive power behavior in the recharge test for a 10.6 km trip with the vehicle battery initially at 100 % load.

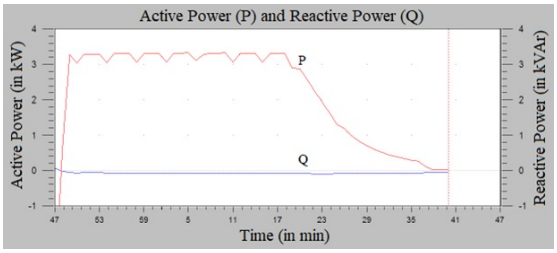

Figure 1: Active and reactive powers - 10.6 km Trip

Tests performed with the available EV indicated that the effects of voltage, current, and power factor throughout the recharging process result in a active power that remains practically constant, followed by a decreasing ramp shown in "Fig. 1". The power rating of the charger determines the maximum demand and the energy supplied is limited by the capacity of the battery bank, with both demand and energy subject to the recharging process efficiency. Thus, the active power curve of "Fig. 1" was transformer in a bar graph with discrete 15-minute time intervals, where the power of final interval has been adjusted to the curve contain all EV charging energy.

3 Deterministic approach of EV's battery charging

"Figure (2) shows, in blue, the typical daily demand curve of two consecutive days (48 hours) of a 75 kVA transformer and, in green, the charging a fleet of 18 EVs simultaneously connected at 1:00 am after traveling the same distance 80 km. According to "Fig. 2", the fleet's charge energy is 305.8 kWh and the total demand reaches 90.5 kW (98.4 kVA). An overload of 31.2 % occurs even the EVs fleet charging starts early in the morning, outside peak hours.

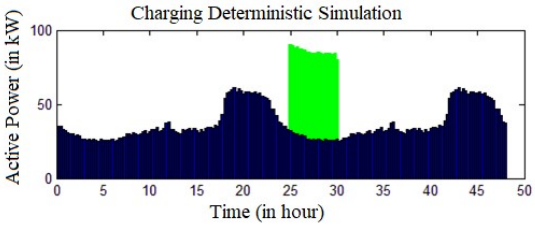

Figure 2: Charging process of deterministic approach

4 Stochastic approach of EV's battery charging

The EVs' charging simulation with different previous distance traveled was performed with different battery charge states. It was considered a lognormal probability density function with a finite value of vehicle autonomy associated with battery capacity [8], that is 100 km. To simulate the battery charging of EVs connected at different times to the transformer load curve was assumed the same number of vehicles, 18, and the same distance traveled by each vehicle, 80 km. In this case the lognormal distribution curve with three parameters was considered, starting at 05:00 pm.

"Figure (3) shows the battery charging demand of the

18 cars, in green, superimposed on the transformer load curve.

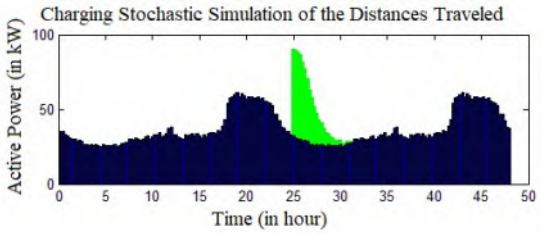

Figure 3: Charging process of stochastic previously distance traveled approach

The simulation of "Fig. 3" reveals a total distance traveled by the fleet equal to 705.8 km, the total EV's fleet charge energy 143.6 kWh and the maximum demand in the transformer 90.5 kW (98.4 kVA). This stochastic simulation presents the same overload as the deterministic case because it has the same number of EVs simultaneously connected at 1:00 am. However, the overload time and the energy consumed was considerably reduced, evidencing a less severe impact on the transformer.

"Figure (4)" shows the battery charging demand, in green, superimposed on the transformer load curve.

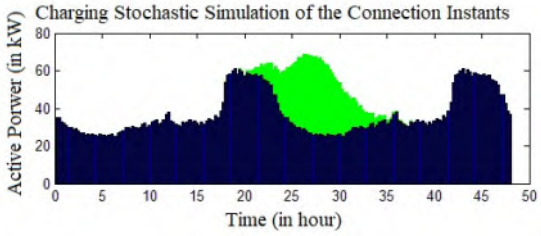

Figure 4: Charging process of stochastic connection moment approach

This simulation of "Fig. 4" presents interesting results. The maximum number of EVs connected simultaneously are two cars, the time of the maximum number of connections is 10:15 pm, the total EV's fleet energy for battery charging is 305.8 kWh and the maximum demand was of 68.7 kW (74.7 kVA) at 2:30 am. In this case, there is no transformer overload indicating that the EV connection instant to the grid is a decisive random variable for the predictions of the demand increase arising from the electric car batteries charging.

Diversity factors (DFs) were defined to compare the deterministic and stochastic simulations results. In order to evaluate the influence of the distances previously traveled (dpt) by EVs during the battery charging process, two diversity factors were considered, DFE, related to total energy, and DFD, related to total distance. Otherwise, to evaluate the influence of the connection at the same time (cst), the diversity factor considered was the DFN, related to number of electric cars simultaneously connected to the grid. "Table 1" shows the results of both variables.

These results reveal a more significant diversity factor related to the number of electric cars that connect at the same time.

Table 1: diversity factors.

	dpt	cst
DFE	47 %	
DFD	50 %	
DFN		11 %

5 CONCLUSIONS

Transforming the EV recharge curve into average demands with conventional measuring ranges allows the superposition of the commonly available demand curves of transformers and feeders. This modification enables deterministic and stochastic analyses to be performed quickly with adequate precision to predict measures to avoid possible overloads. The decisive importance of EV's connection moment for charging the batteries, in order to avoid exceeding the capacity of elements of the network, demonstrated that it is advisable to provide automatic communication to take advantage of existing off-peak hours, offering more affordable tariffs within the framework of smart energy grids.

References

[1] ITAIPU BINACIONAL and KWO GIMSELSTROM. Electric vehicle. Technical report, 2011.

[2] C. Dustmann. Advances in zebra batteries. *Journal of Power Sources*, 127:85–92, 2005.

[3] J.E. Freund and I. Miller. Probability and statistics for engineers. *Prentice Hall*, 1965.

[4] J V. Serra F.M.F. Particewlli L.A Pecorelli Peres, J. F. M. Pessanha. Infrastructure plan for charging stations for electric vehicles in rio de janeiro. In *Electric Vehicle Synposium 26 – EVS 26*, Los Angeles, California, 2012.

[5] L. A. Horta Nogueira L.A Pecorelli Peres, G. Lambert Torres. Analisys and discussion on energy supply to non-road electric vehicles in brazil. In *IEEE Power Engineering Society - TD Latin America Conference*, São Paulo, SP, 2002.

[6] Marcus. L. P. Peçanha A B. Neto David T. da Silva M. Beatriz M. P. Medeiros L.A Pecorelli Peres, J. F. M. Pessanha. Test procedures and measurements for recharge evaluation of battery electric vehicles in power concessionaires in brazil. In *Electric Vehicle Synposium 24 – EVS 24*, Stavanger, Norway, 2009.

[7] J. Larminie J.; Lowry. *Electric Vehicle Technology Explained.* John Wyley Sons, Ltd, 2003.

[8] JacKbsson N. Plötz P. and Frrances S. On the distribution of daily travel distances. *Transportation Research, Part B: Methodological*, 101:213–227, 2017.

COMPARATIVE ANALYSIS OF BLAST FURNACE COOLER SYSTEM PERFORMANCE WITH DIFFERENT PRESERVATION TECHNIQUES AND DESIGN CONDITIONS

Author: Eustáquio Vieira Júnior[1] *juniorevj@gmail.com*
Advisor(s): Norberto Mangiavacchi[1]
[1] Rio de Janeiro State University

August 05, 2020
PPG-EM Seminars: season **2020**
http://www.ppgem.uerj.br

Keywords: Blast Furnace, Stave Cooler, Fluid Dynamics, Computational Fluid Dynamics.

1 Introduction

The Ternium Brasil stellmaking company, in Rio de Janeiro, operates two blast furnaces. These two equipments have the same production capacity and their operations started in 2010. The stack cooler systems of the Blast Furnaces are stave coolers, and the hearths are jacket coolers. The representation of Blast Furnace arrangement is shown in Figure.1.

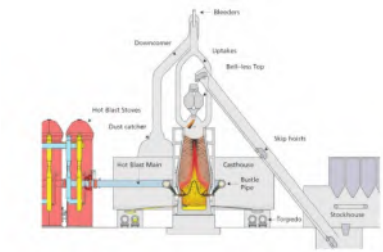

Figure 1: Example of Blast Furnace general arrangement, from [2]

Several operational instabilities occurred in the beginning of operation that were exarcebated by unprogrammed operational stoppages. These stoppages brought consequences for the Blast Furnaces, and directions to preserve these equipments were established. The objective of these actions were to restore the operational conditions and extend the Blast Furnaces and the ancillary equipments service lives. The information about the Blast Furnaces of Ternium Brasil are shown in Tab. 1

The Ternium Brasil Blast Furnaces have Cooper Stave Coolers between the fisrt row of the bosh and the forth row in the inferior stack. The stave coolers from fifth row up to eight row, localized in superior stack, are made of cast iron.

There are many maintenance techniques that are used to preserve the cooling capacity of staves cool. Among these, the Ternium preservation team executes:

Table 1: Main characteristics of Ternium Brasil Blast Furnace 2.

ITEM	BF2
Internal Volume	3284m^3
Work Volume	2775m^3
Hearth Diameter	12,0m
Production Capacity	7500t/day
Quantity of Tap Holes	2
Quantity of Tuyeres	32
Burden Distribution Type	Bell Less Top
Slag Granulation Type	INBA
Maximum Blast Temperature	1250°C
Stack, Belly and Bosh Cooler System	Stave Coolers
Hearth Coolers System	Jacket Coolers
Start of Service Life	16/12/2010

- Repare the cooling line by welding process;
- Introduce flexible pipes into the damaged cooling lines;
- Insert cigar coolers to recr, partially, the stave cooler systems.

In this work the evaluation of these preservation techniques regarding the fluid dynamics behavior and the thermal consequences in the stave cooler bodies are presented. Among these consequences, it is important to know whether the stave coolers reach the mechanical limits of the materials employed in their fabrication.

2 The Mathematical Model And Numerical Method

The methodology used to analyse the fluid flow and heat transfer in the stave coolers was a Finite Element Computational Fluid Dynamics (CFD) model. The governing equations are the continuity, Eq. 1, momentum,

Eq. 2, and energy, Eq. 3 balance equations (Pontes and Mangiavacchi 3). :

$$\frac{\partial \rho}{\partial t} + \nabla \rho \cdot v = 0 \tag{1}$$

$$\frac{\partial v}{\partial t} + v \cdot \nabla v = -\frac{1}{\rho}\nabla p + \nu \nabla^2 v + g \tag{2}$$

$$\frac{\partial T}{\partial t} = \alpha \cdot \nabla^2 T + \frac{Q}{\rho \cdot C_v} \tag{3}$$

The CFD software used is Ansys Fluent ®. The first stage in the modeling was to define the domain geometry. In this case, it was necessary to create the geometric model of the stave coolers, the flexible hoses and the cigar coolers. The second stage, after the definition of the domain geometries, was the mesh construction. In this stage, we choosed to make the mesh using the internal Ansys Fluent ® mesh generator [1].The third stage, after the mesh defined, was the datas insertion to solve the problem in analyse. The fourth stage, after the solution converged, was to check the balances of mass and energy with the objective to verify if the Continuity in EQ.1, Momentum in EQ.2 and Energy in EQ.3 balances are satisfied.

3 Computational Results and Discussion

After the balances were checked, and the results were satisfatory, graphic plots with temperature contour curves were created and were employed to analyse the performance of fluid flow and stave cooler heat transfer after the maintenance actions. The results are evidenced in Fig.2, Fig.3 e Fig.4.

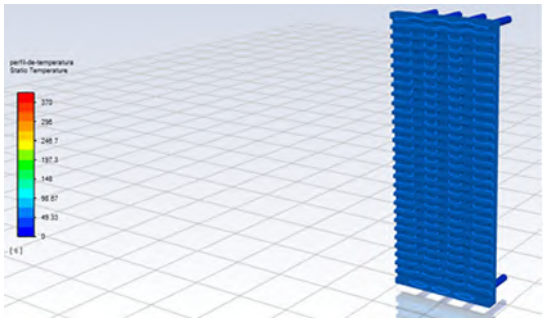

Figure 2: Stave Cooler in design condition

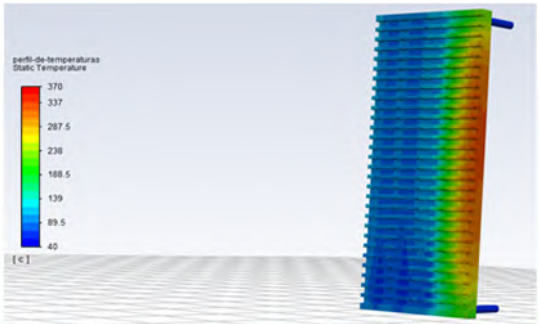

Figure 3: Stave Cooler with one side cooler line damaged

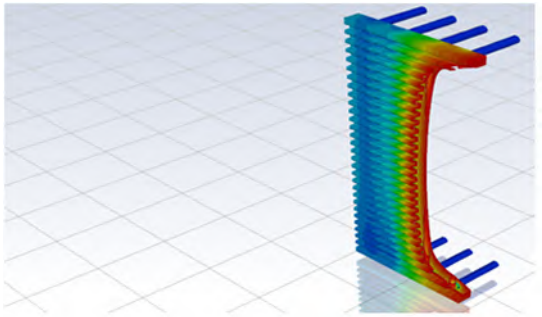

Figure 4: Stave Cooler with two lines damaged

Based on the analysis of the temperature contours, we can draw conclusions about the performance of stave coolers that received maintenance actions. The most important conclusion, as seen on the images above, is that the staves can not stay without regrigerated fluid for long time because this can cause severe damages in the stave bodies. And these damages can bring serious problems with the structure stability of the blast furnace shell. Analysis considering the performance of the cigar coolers will be also discussed.

4 Conclusions

Based on the analysis of the temperature contours, we can draw conclusions about the performance of stave coolers that received maintenance actions. The most important conclusion, as seen on the images above, is that the staves can not stay without regrigerated fluid for long time because this can cause severe damages in the stave bodies. And these damages can bring serious problems with the structure stability of the blast furnace shell. Analysis considering the performance of the cigar coolers will be also discussed.

5 Acknowledgments

The authors would like to acknowledge financial support from FAPERJ, CNPq, CAPES, and TERNIUM..

References

[1] Inc. Ansys. *ANSYS Fluent User's Guide*. Canonsburg, PA, release 2020r1 edition, 2020.

[2] Hisko Toxopeus Maarten Geerdes, Cor van der Vliet and Fernando Tadeu Pereira de Medeiros. *Modern Blast Furnace Ironmaking an introduction*. Netherlands, 2 edition, 2009.

[3] J. Pontes and N. Mangiavacchi. *Fenômenos de transferência com aplicações às ciências físicas e à engenharia*. SBM, Rio de Janeiro, 2016.

IN VITRO TESTS TO ANALYZE THE INFLUENCE OF COPPER-BASED SEALANTS APPLIED ON THERMOPLASTIC POLYMERS OBTAINED BY 3D PRINTING IN THE REPRODUCTION OF HOSPITAL BACTERIA

Author: Fernanda Torres[1] *souza.fernand@posgraduacao.uerj.br*
Advisor(s): Norberto Mangiavacchi[1]
[1] Rio de Janeiro State University

August 12, 2020
PPG-EM Seminars: season **2020**
http://www.ppgem.uerj.br

Keywords: Copper Based Sealants, In Vitro Tests, additive manufacturing.

1 Introduction

The use of Copper in medicine as an antimicrobial agent continued until the appearance of the first commercial antibiotics in 1932, falling into disuse[6]. The oldest medical record cited of the use of copper was found in an ancient Egyptian papyrus, dated from 2600 to 2200 B.C., which details the use of copper to sterilize wounds and to containers with drinking water[2]. Currently, with the emergence of more resistant bacteria and the emergence of new types of viruses, the need for greater protection and further research and studies on the use of Copper has been realized[3]. Environmental surfaces in hospitals are increasingly being recognized as possible reservoirs for health-associated pathogens that can be transmitted to patients, for example, through dirty hands, contaminated medical equipment or direct interactions with the environment by a patient can become contaminated[1]. touching the contaminated surfaces and then transferring the microorganisms to other patients, directly or indirectly, contaminating other surfaces[5].

With this we will study in vitro tests to analyze the influence of sealants based on Copper applied on thermoplastic polymers obtained by 3D printing in the reproduction of hospital bacteria.[5] It is known that under specific conditions, Copper can eliminate microbes or prevent their further growth. Under conditions when they were in contact with Cooper, already were Survival rates of 0% were obtained in some microbes. However, still with few studies on its performance in the form of paints and sealants on some types of bacteria and viruses present specifically in a hospital environment[4].

2 Objective

For this work, Copper-based sealants or paints that can be applied simply on thermoplastics and additionally, and evaluate the time of effectiveness of these paints, analyzing the growth of some bacteria more common in hospital environments, roughness and wettability of the Copper-based sealant and the growth of these cultures in this sealant over the thermoplastic, analyzing the survival rate of these cultures compared to the first growth.

3 Materials and methods

The methodology for some of the main stages of the project will be:

Measures roughness already performed on the PLA plates showed mean roughness values (Ra) of 22.51 micrometers 8.40 in a direction parallel to the preferred PLA guidance lines obtained by printing 3D and 8.72 micrometers 3.49 in a direction perpendicular to these lines, which characterizes orientation preferred surface area. The other trials are in progress.

i) Chemical and morphological characterization of surfaces and seal coatings using optical microscopy (MO), scanning electron microscopy (SEM) and semi-quantitative chemical analysis by EDS (Energy Disperive Spectroscopy);

ii) Quantitative characterization of coatings and colonies of bacteria adhered to In Vitro Tests through analysis techniques and digital image processing (PDI);

iii) In vitro tests that simulate the growth environment of bacteria and viruses in the hospital environment;

iv) Tests of duration of the effectiveness of the sealing coatings through cleaning re-use of surfaces already tested;

v) Statistical analysis of the results obtained.

3.1 Parameters

i) Material: polylactide (PLA);

ii) Temperature: 210°;

iii) Print speed: 35 mm/s;

iv) External wall printing speed: 17.5 mm/s;

v) Print speed of the first and last layer: 17.5 mm/s;

vi) Layer height: 0.3 mm;

vii) Line width: 0.48 mm;

viii) Number of walls: 2;

ix) Base layers: 3;

x) Top layers: 3;

xi) Filling density: 10

Figure 1: Thermoplastic (PLC) obtained by 3D printing

4 Results

The expetected results of this project are:

- Roughness analysis of the PLA material before and after the use of sealant;
- Statistical and comparative data on bacterial growth;
- Effectiveness in combating copper as an antibacterial;
- Bibliographic survey and preparation of a technical-scientific report equipped with methodology and that serves as an instrument for the characterization for samples covered with sealants;
- Mastery of characterization techniques on macro, micro and nano scales for protective sealing coatings;

5 Conclusions

In Addition this work intends to confirm previous studies with the use of Copper as an antimicrobial tested in hospitals, to verify the effectiveness of this material, possible toxicity, manufacture and use of another barrier against hospital bacteria, being in the future a possibility for further studies, fabrications, or alterations with other types of materials with the use of this sealant whose initial idea is to open studies between engineering and the health area.

6 Acknowledgments

This work was carried out with the support of the Coordination of Improvement of Higher Education Personnel-Brazil (CAPES),the advisor of this research Ph.D. Norberto Mangiavacchi, the co-advisor D.Sc. Marilia Diniz, the D.Sc. Daniel José Nahid Mansur Chalhub, partnership with the Laboratory of Microbiology at the UFRJ.

References

[1] Marilia Garcia Diniz, Marco Antonio Santos Pinheiro, Antonio Carlos Canabarro Andrade Junior, and Ricardo Guimarães Fischer. Characterization of titanium surfaces for dental implants with inorganic contaminant. *Brazilian oral research*, 19(2):106–111, 2005.

[2] B Liliana España-Sánchez, J Alberto Rodríguez-González, Pablo González-Morones, M Guadalupe Neira-Velázquez, Bernardo Franco-Bárcenas, Fernando Anaya-Velázquez, Claudia Leticia Mendoza-Macías, Carlos A Ávila-Orta, and Felipe Padilla-Vaca. Nanocompuestos de polipropileno con nanopartículas de cobre: preparación, activación superficial por plasma y actividad antibacteriana. *Acta Universitaria*, 24(3):13–24, 2014.

[3] Gregor Grass, Christopher Rensing, and Marc Solioz. Metallic copper as an antimicrobial surface. *Applied and environmental microbiology*, 77(5):1541–1547, 2011.

[4] Humberto Palza, Mauricio Nuñez, Roberto Bastías, and Katherine Delgado. In situ antimicrobial behavior of materials with copper-based additives in a hospital environment. *International journal of antimicrobial agents*, 51(6):912–917, 2018.

[5] Vanda Ferreira Ribeiro. Desenvolvimento de compósitos antimicrobianos a base de sebs/pp aditivados com partículas de cobre. 2019.

[6] Chufeng Sun, Yi Li, Zhi Li, Qiong Su, Yanbin Wang, and Xuqing Liu. Durable and washable antibacterial copper nanoparticles bridged by surface grafting polymer brushes on cotton and polymeric materials. *Journal of Nanomaterials*, 2018, 2018.

DEVELOPMENT OF A TRANSIENT HEAT TRANSFER MATHEMATICAL MODEL FOR CALCULATING THE TIME CONSTANT OF PHOTOVOLTAIC SOLAR PANELS

Author: Hugo Leonardo Ribeiro Baptista de Souza[1] *hugoleonardor@hotmail.com*
Advisor(s): Manoel Antônio da Fonseca Costa Filho[1]
[1] Rio de Janeiro State University

PPG-EM Seminars: season **2020**
http://www.ppgem.uerj.br
Aug 12, 2020

Keywords: Solar energy, transient heat transfer, PV modules, renewable energy

1 Introduction

The temperature of the photovoltaic solar panels is one of the parameters that most influence the performance of the solar power generation systems, impacting adversely on their performance. Thus, several studies have recently been carried out to calculate the temperatures for these equipments, allowing an efficiency estimate based on empirical correlations. However, in the thermal modeling of the panels, it is usual to consider them in steady state, with the premise that the high thermal inertia of the equipment makes the changes in its temperature, with momentary variations in solar radiation, to be negligible. For a more accurate verification of the performance of these systems, it is necessary to study the temperature behavior of the panels when subjected to sudden variations in external variables, considering a transient model of heat transfer, little explored in the literature. In this work, a mathematical model of transient heat transfer is developed and solved numerically, in order to calculate the time constant of photovoltaic solar panels, which here is the time necessary for 63% of the total temperature variation to occur after the instant when there was a sudden change in solar radiation. Then, the time constant calculated will be compared with its measured value from the solar panels located in the building of the Mechanical Engineering Graduate Program at UERJ.

2 Methodology

The following components are relevant to the problem of heat transfer in a photovoltaic solar panel:

- Highly transparent glass covering
- EVA layer
- Photovoltaic solar cells
- Another EVA layer
- Backsheet

To determine the temperature distribution on the panel, the unidimensional heat conduction equation must be solved for each layer, considering the respective thermophysical properties:

$$\frac{\partial^2 T}{\partial x^2} = \frac{\rho C_p}{k}\frac{\partial T}{\partial t} \tag{1}$$

with the following boundary condition for the front surface, exposed to the sun:

$$-k\frac{\partial T}{\partial x} = G(\tau\alpha - \eta) - (q_{convf} + q_{radf}) \tag{2}$$

and the following boundary condition for the rear of the panel:

$$k\frac{\partial T}{\partial x} = q_{convr} + q_{radr} \tag{3}$$

where G is the solar irradiance, τ is the transmittance, α is the absorbance and η is the module efficiency, which is function of the temperature and depends on the model of the solar panel. The material properties are assumed as constants. It's assumed that there is no heat generation (heat dissipation from the solar cells through Joule's effect is negligible) and that the heat transfer on the surfaces other than the rear and the front are negligible, because of their small area.

In order to find the temperature distribution along all the panel, it's also necessary to define the boundary conditions for the interface of the layers.

For the next step, it's necessary to solve the steady state problem, considering the new value for the solar irradiation, after the sudden change mentioned in the introduction. Then, considering the average temperatures of the panel for the transient and for the steady state problem, the time constant will be the time that satisfies the following relation:

$$\frac{T_a(t) - T_a(0)}{T_a(\infty) - T_a(0)} = 0,63 \tag{4}$$

where $T_a(t)$ is the average temperature of the panel on the instant t, $T_a(\infty)$ is the average of the temperatures obtained by solving the steady state problem, and $T_a(0)$

is the average temperature of the panel on the instant $t = 0$.

3 Conclusions

The solution of the presented equations allows the calculation of the theoretical time constant for the panel, which must be compared with the experimental result in order to validate the model.

References

[1] S. Armstrong, W.G. Hurley. A thermal model for photovoltaic panels under varying atmospheric conditions. Galway, Ireland, 2010.

[2] M. Akhsassi, A. El Fathi, N. Erraissi, N. Aarich, A. Bennouna, M. Raoufi, A. Outzourhit. Experimental investigation and modeling of the thermal behavior of a solar PV module. Marrakech, Morocco, 2018.

[3] Incropera, F. P. Fundamentals of heat and mass transfer. John Wiley, Hoboken, New Jersey, USA, 2007.

DEVELOPMENT OF THE TYPICAL METEOROLOGICAL YEAR (TMY) FOR THERMAL SIMULATION OF BUILDINGS FOR THE VILA MILITAR METEOROLOGICAL STATION IN THE CITY OF RIO DE JANEIRO

Author: Marcelo Fernandes Melo Monteiro[1] *marcelofmm@gmail.com*
Advisor(s): Manoel Antônio da Fonseca Costa Filho[1]
[1] Rio de Janeiro State University

PPG-EM Seminars: season **2020**
http://www.ppgem.uerj.br
September 18, 2020

Keywords: Energy, efficiency, HVAC, TMY.

1 Introduction

The metropolitan region of Rio de Janeiro has the land use characteristics with a high percentage of areas covered with asphalt and concrete are able to convert and store solar radiation into a greater extent than rural areas a high population density. The high degree of industrialization a large concentration of pollutant emissions and heat sources promoting the onset of a horizontal temperature gradient phenomenon known as the urban heat island [2]. This manuscript aims to develop the Typical Meteorological Year (TMY) using data from the Vila Militar meteorological station located in the city of Rio de Janeiro. From the processing of weather data for the period from 2007 to 2019, the TMY produced will be used in the energy simulation of buildings and thermal load projects in HVAC systems.

2 Materials and Methods

A typical meteorological year (TMY) data sets are used by building designers for modeling renewable energy conversion systems. TMY data set provides users with a annual data set that holds hourly meteorological values that typify conditions at a specific location over a period of time. TMY data have natural diurnal and seasonal variations and represent a year of typical climatic conditions for a location, however not designed to provide meteorological extremes [3]. TMY data sets are formed by the 12 months of the year and contain real time series meteorological measurements with hourly records that are combined without modification to form a single year with a serialized data record for primary measurements. They can also contain filled or interpolated data for periods when the original observations are missing from the data file [3].

The 12 typical months selected were chosen using statistics determined using the Sandia method, which has an empirical approach that selects individual months from different years that occurred in the registration period. In this study, four elements were considered: direct global radiation, dry bulb temperature, dew point temperature and wind speed. These elements are considered the most important to simulate solar energy conversion systems and construction systems. The algorithm attaches greater importance to the solar radiation of the selected months, thus, the months may not be typical for other meteorological characteristics. Wind speed was used in the selection of typical months, but its weight is relatively low in relation to the other elements, which prevents it from being typical enough to simulate wind energy conversion systems [3].

The Vila Militar meteorological station belongs to the Instituto Nacional de Meteorologia (INMET). It is located at -22.861389 latitude, -43.411389 longitude and an altitude of 30.43 meters. This station measures and records temperature, humidity, pressure, precipitation, radiation, wind speed and direction at intervals of 1 in 1 hour [1]. The meteorological data sets used for the calculations may contain missing values. The method used to fill in missing data was recommended by ASHRAE. Gaps of up to 6 hours were filled by linear interpolation to provide the most complete time series possible. When data is missing at the right time, they can be replaced with data up to 0.5 hours before or after, when available. Microsoft Excel was used for data processing.

3 Results

The period analyzed in Vila Militar was from 2007 to 2019. Looking at Figure (1), the year with the most selected months was 2015, with three months. The years 2007, 2009, 2013, 2017 and 2019 had no selected months. The selected months were not concentrated in short periods of time, as there is a diversification of the months in practically the entire period studied.

4 Conclusions

The metropolitan region of Rio de Janeiro has great influence from the sea and the massifs that surround the city. Thus, we were able to identify several microclimates that should be studied in order to have more detailed and precise data for energy efficiency projects.

TMY	
January	2018
February	2015
March	2015
April	2014
May	2012
June	2015
July	2016
August	2014
September	2011
October	2016
November	2008
December	2010

Figure 1: TMY from Vila Militar weather station

The creation of the typical meteorological year (TMY) of several regions allows the identification of these microclimates and the impact on energy efficiency projects.

References

[1] INMET. Intituto nacional de meteorologia. Technical report, https://portal.inmet.gov.br/, 2019.

[2] R. B. Stullr. *An Introduction to Boundary Layer Meteorology*. Kluwer Academic, 1993.

[3] S. Wilcox and W. Marion. Users manual for tmy3 data sets. Technical report, National Renewable Energy Laboratory, 2008.

VARIATIONS OF AINV AND THEIR BLOCK VERSIONS

Author: Julia Sekiguchi da Cruz[1] *julia-seki@hotmail.com*
Advisor(s): Luiz Mariano Carvalho[1]
[1] Rio de Janeiro State University

August 19, 2020
PPG-EM Seminars: season **2020**
http://www.ppgem.uerj.br

Keywords: Approximate inverse, linear system, preconditioner, block matrices.

1 Introduction

In several areas of science and industry we need to solve sparse and large linear systems of the form $Ax = b$, where $A \in \mathbb{R}^{n\times n}$ is a nonsingular matrix, $b \in \mathbb{R}^n$ is the right-hand side and $x \in \mathbb{R}^n$ is the solution vector. They can only be solved using iterative methods like Conjugate Gradients, GMRES, BICGSTAB, etc. However, iterative methods also may have slow convergences for large problems, and for that reason preconditioners are used. Preconditioners have the objective of transforming one linear system into another with the same solution but easier to solve. One type of preconditioner is the matrix M that approximates the inverse of the matrix A, that is $M \approx A^{-1}$. In this case, the preconditioned system is like $MAx = Mb$ or $AMy = b$, such that $x = My$. The present work is based on the study of preconditioner AINV ("Approximate Inverse"), formulated by Benzi and Tuma [3], in 1996, which calculates the approximate inverse factorization of non singular, large and sparse matrices. We analyze the main variations of AINV found in the literature and propose their adaptations for block matrices.

2 Main idea of AINV

The AINV method produces a factorization of the approximate inverse of A using A-biorthogonalization. The main idea is to produce matrices Z, W and D that $A^{-1} \approx ZD^{-1}W^T$, where Z and W are nonsingular and D is a diagonal nonsingular matrix, that is

$$W^TAZ \approx D = \begin{bmatrix} d_{11} & 0 & \cdots & 0 \\ 0 & d_{22} & \cdots & 0 \\ \vdots & \vdots & \ddots & \vdots \\ 0 & 0 & \cdots & d_{nn} \end{bmatrix}.$$

The scalars d_{ii} are called pivots. The A-biorthogonalization process is applied to linearly independent initial vectors chosen as being $z_i^{(0)} = e_i$ and $w_i^{(0)} = e_i$ and, for this reason, Z and W are upper triangular matrices.

As Z and W tend to be dense, it is computationally impracticable to execute AINV process for large matrices. To deal with this problem we drop some entries of Z and W during the process, to make them sparse. Because of the drop, it is possible that the algorithm produces zero pivots. If this occurs, the process cannot be completed and we say that the algorithm has "broken".

3 Contributions

In this section, we show the main contributions of this work.

3.1 Article published on Linear Algebra and its Applications

In this section, we describe the article published on Linear Algebra and it Applications. In this work, we provided a mathematical treatment to AINV for block matrices, named BAINV. BAINV was originally proposed by Benzi, Kouhia and Tůma [5] for symmetric matrices. We consider that A is a nonsingular symmetric matrix with block structure, where the blocks are of the order $b \times b$, where n is divisible by b. If $N = \frac{n}{b}$, we say that A is a $N \times N$ block-matrix. As A is symmetric, the approximate inverse factorization is of the form $A^{-1} \approx ZD^{-1}Z^T$, where we consider that Z, and D also have block structure, with block size b. In this case, the pivots D_{II} are the $b \times b$ block diagonals of D and the process breaks when D_{II} is singular for some $1 \leq I \leq N$. First, we demonstrated the consistency of BAINV, given by Lemma 1 and Theorem 2.

Lemma 1. *As long as block A-orthogonalization algorithm does not break (i.e., singular D_{II}'s are not generated), it yields an upper block-triangular Z. Furthermore, its block-diagonal is comprised of identity blocks.*

Theorem 2. *Let A be a symmetric $N \times N$ block-matrix such that $A_{1:J,1:J}$ is nonsingular for $J = 1, 2, \ldots, N$. Then block A-orthogonalization algorithm does not break and returns a nonsingular block-diagonal matrix D and a nonsingular block-matrix Z such that $A^{-1} = ZD^{-1}Z^T$ (or, equivalently, $Z^TAZ = D$).*

We also prooved that BAINV does not break for M and H matrices, as we can see on Theorems 3 and 4.

Theorem 3. *Let $A \in \mathcal{M}$ (a M-matrix) be an $N \times N$, symmetric, nonsingular block-matrix. Then BAINV*

algorithm does not break, as it yields blocks D_{II} which are nonsingular M-matrices.

Theorem 4. *Let the block-matrix A be a symmetric H-matrix with positive entries in its main diagonal and such that the comparison matrix $C(A)$ is a nonsingular M-matrix. Then BAINV algorithm does not break, as it yields blocks D_{II} which are nonsingular H-matrices.*

3.2 Taxonomy

In this work, we study the main properties and variations of AINV found in the literature.We analyzed the most significant characteristics of these methods as the dropping strategy, proceeds to avoid breakdown and relations between approximate inverse factor with LDU factors of A. We also evaluated the complexity of each variation. Thereby, they were classified into four classes:

- AINV Class - contains the variations that are closer to the original AINV. The main differences among them are the A symmetry, dropping strategies, and pivot calculation;
- FFAPINV Class - in this class, the Z vectors are used to calculate W entries and, similarly, the W vectors are used to calculate Z entries;
- LU Class - the approximations of the L and U factors of A are calculated using AINV;
- Pivoting Class - complete pivoting is carried out during the algorithm in order to avoid breakdown or improving the quality of the preconditioner.

3.3 Block Versions

Several variations of AINV have been developed, but a few versions for block matrices have been proposed. They are:

1. Bridson and Tang [6], in 2000, presented a version based on FFAPINV.
2. Benzi, Kouhia and Tůma [5], in 2001, presented a symmetric version for problems from mechanics of solids.

Some of the main motivations of working with block matrices are: stability and improved computational performance; preservation of physical aspects of the problem that are associated with the matrix block structure. In this work, we adapted some scalar AINV variations to block matrices, developing their supporting mathematical theory. They are:

- AINV-NS [1] - is the original AINV for non symmetric matrices;
- SAINV-NS [4] - the pivots are differently calculated to avoid breakdown, when A is positive definite;
- SAINV-VAR [8] - SAINV is used to obtain W, D and U. Z is obtained using the relation $Z = U^{-1}$, where U^{-1} is estimated by Neumann series. A is positive definite.
- RIF [2] - SAINV is used to obtain the approximations of LDL factors of A, where A is symmetric.
- RIF-NS [7] - SAINV is used to obtain the approximations of LDU factors of A, where A is non symmetric.

4 Conclusions

We present the final considerations below:

- We analyzed the main variations of scalar AINV and developed a supporting mathematical theory to their block versions.
- We are implementing the methods from Taxonomy and Block Versions, using C++ and Python languages;
- As a future work, we will make a broad comparison of the variations of AINV, including the comparison with other preconditioners and analyze their respective numerical and computational performances;

References

[1] M. Benzi and M. Tůma. A sparse approximate inverse preconditioner for nonsymmetric linear systems. *SIAM Journal on Scientific Computing*, 19: 968–994, 1998.

[2] M. Benzi and M. Tůma. A robust Preconditioner with low memory requirements for large sparse least squares problems. *SIAM Journal on Scientific Computing*, 25:499–512, 2003.

[3] M. Benzi, C. D. Meyer, and M. Tůma. A sparse approximate inverse preconditioner for the conjugate gradient method. *SIAM Journal on Scientific Computing*, 17:1135–1149, 1996.

[4] M. Benzi, J. K. Cullum, and M. Tůma. Robust Approximate Inverse Preconditioning for the Conjugate Gradient Method. *SIAM Journal on Scientific Computing*, 22:1318–1332, 2000.

[5] M. BENZI, R. KOUHIA, and M M. TŮMA. Stabilized and block approximate inverse preconditioners for problems in solid and structural mechanics. *Computer Methods in Applied Mechanics and Engineering*, 190:6533–6554, 2001.

[6] R. Bridson and W. Tang. Refining an approximate inverse. *Journal of Computational and Applied Mathematics*, 123:293–306, 2000.

[7] A. Rafiei and M. Bollhöfer. Robust incomplete factorization for nonsymmetric matrices. *Numerische Mathematik*, 118:247–269, 2011.

[8] A. Rafiei and F. Toutounian. New breakdown-free variant of ainv method for nonsymmetric positive definite matrices. *Journal of Computational and Applied Mathematics*, 219:72–80, 2008.

PUBLIC POLICIES TO ENCOURAGE PHOTOVOLTAIC GENERATION

Author: Saldanha, MM[1] *mmendessaldanha@gmail.com*
Advisor(s): Costa Filho, MAF[1]
[1] Rio de Janeiro State University

PPG-EM Seminars: season **2020**
http://www.ppgem.uerj.br
Sep 28, 2020

Keywords: Renewable energy. Public policies. Tariff feed-in. Solar energy .

1 Introduction

Solar energy is a clean and renewable source, researchers are looking for clean sources to protect the environment from pollution. Global warming is increasing every day, as scientifically proven, fossil sources of energy contribute a lot to this increase. Brazil has a high solar radiation index in relation to most other countries, so there is great opportunity for the use of solar energy in the Brazilian territory. It is therefore important to contribute to the Legislative Power to find legal ways to encourage the generation of photovoltaic energy in Brazil. This work is a continuation of the research initiated with Bruno Campos' essay[3].

2 Concepts

Solar radiation can be used as a source of thermal energy for heating fluids and environments and for generating mechanical or electrical power, or even when focusing on certain materials, it produces thermoelectric or photovoltaic effects. The thermoelectric effect is characterized by the rise of an electromotive force, in a circuit formed by the junction of two different metals, under specific conditions. In the photovoltaic effect, the photons contained in the sunlight are converted into electrical energy, through the use of solar cells.

3 World Solar Energy Outlook

According to Renewables 2020 Global Status Report (REN2, 2020), the global solar energy market has increased by 44 percent. China has had a substantial decline, but continues to dominate the world market for equipment manufacturing and technological advances. According to a survey carried out by Renewables 2020 Global Status Report (REN2, 2020), this year, solar photovoltaic energy was responsible for 10.7 percent of the total generation in Honduras, Italy 8.6 percent (actions were applied in this country), Germany 8.2 percent, Greece 8.3 percent, Chile 8.1percent. By the end of the year, the solar energy capacity will be sufficient to produce around 2.8 percent of the global electricity generation. At the end of 2019 the leading countries in accumulated energy generated through photovoltaic panels were China, the United States, Japan, Germany and India. In most countries, there is still a need to improve and/or implement public policies to encourage photovoltaic generation.

4 Solar Energy Panorama in Brazil

Currently, the two most used sources in Brazil are hydraulic and oil, according to data collected by ANEEL - National Electric Energy Agency - Atlas of Electric Energy of Brazil - 3rd Edition 2008, about 75.68 percent of electric energy comes from hydraulic generation, due to the shortage of supply and socio-economic problems [1]. It will be necessary to take advantage of alternative sources, also aiming to reduce the negative impacts on the environment and society. In Brazil, the use of solar energy has been directed through photovoltaic systems for electricity generation, targeting isolated communities from the electricity grid and regional development. From the new perspective of national energy policy, new projects can bring electricity to thousands of Brazilian communities and households. The PDE - Decennial Plan for the Expansion of Energy 2030 in Brazil, mentions the increased participation of wind and solar sources, 11 percent solar in 2012, 15 percent in 2021 and 16 percent in 2030. In 2019, the PDE - Decennial Energy Expansion Plan 2030 in Brazil, concluded that with the change in the matrix composition (less hydroelectric participation and greater competitiveness of variable renewable sources), expansion is necessary to guarantee the power capacity.

5 Existing incentives to solar energy

The regulation of Law no. 10.295, of 17th October, 2001, which provides for the Conservation and Rational Use of Energy National Policy, was the driving force behind this technology. The ANEEL 482/2012 normative resolution was a great existing incentive to solar energy, allowing consumers to install small generators in their homes. The surplus energy will be injected into the network, in exchange for credits, and can be used within 36 months, this incentive is called net metering. The "Luz para Todos" program, implemented in 2003 by the Ministry of Mines and Energy,

made possible to install several photovoltaic systems in communities in the interior of the country that do not have access to electricity and are not part of the National Interconnected System (SIN). The Normative Resolution no. 77/2004 established that incentive generation projects (energy from renewable sources) are entitled to a 50percent, 80 percent or 100 percent discount on transportation tariffs, TUSD / TUST (Tariff for the Use of Distribution Services / Tariff for Use of Transmission Services)[2]. The National Electric Energy Agency - ANEEL on 9/12/2001 authorized the self-producers and solar energy producers to directly sell surplus energy to special consumers, with a load between 500 KW and 3,000KW, without the intermediation of the distributors. CONFAZ - National Council for Tax Policy, agreement no. 101/1997, exempt from ICMS (Tax on Circulation of Goods and Services) operations with equipment for the generation of solar energy by photovoltaic cells. REIDI - Incentive Scheme for the Development of Infrastructure that suspends the Contribution to the Social Integration and Formation of the Civil Servants' Heritage Program (PIS / PASEP) and the Contribution to the Financing of Social Security, in cases of sale or import of machinery and equipment for the operation of infrastructure works for solar energy generating plants. The income tax exemption on the issuance of a debt security "Incentive Debentures" for investment purposes for the implementation of projects for the generation of solar energy. PADIS - Semiconductor Industry Technological Development Support Program that grants income tax exemption and reduces the contribution rates to PIS / PASEP, CONFINS and IPI to zero, instituted by articles 1 to 11 of Law 11.484 , of 31st May, 2007. The Computer Law provides tax incentives to companies that invest in Research e Development (R e D) in priority areas such as smart cities, including the production of equipment for the generation of solar energy. Income Tax Reduction for projects implemented in the SUDAM - Superintendence for Development of the Amazon and SUDENE - Superintendence for Development in the Northeast, which cover the main Brazilian regions in terms of solar radiation. Reserve Energy Auctions (LERs), in December 2017 a New Energy Auction was held, including the photovoltaic solar source that contracted around 600MW. Brazilian Photovoltaic Labelling Program (PBE) / INMETRO - Directive 4/2011 - quality, safety and energy efficiency for imported national products. Since 2015 Caixa Econômica offers a credit line for the acquisition of photovoltaic energy equipment, so called Construcard financing. PROESCO - Support for Energy Efficiency projects, this program was created by BNDES in 2006 and in 2008 it accredited Bradesco S.A. to act as a mandatory financial agent, financing projects in the energy efficiency sector in the country. Climate Fund is a program created by the Law 12.114 on 09.12.2009, regulated by Decree 10.143, of 28.11.2019, of the BNDES, being an instrument of the National Policy on Climate Change, with the objective of supporting the implementation of businesses related to the reduction of greenhouse gas emissions. Inova Energia is a joint action plan made available by BNDES, the National Electric Energy Agency (Aneel), and the Financier of Studies and Projects (Finep), which aim to support Brazilian companies in the development of technology for equipment used in the field of renewable energy such as photovoltaic solar.

6 Comparative analysis of public policies presented in Brazil

Brazil is going through a period of significant reforms in the electric sector, the government presents a set of tax incentives, financing and labelling, in particular for the photovoltaic source. These measures may be applied in isolated systems, not connected to the electric network, being of great importance for rural areas and borders.

7 Improvements to existing incentives in Brazil

The government needs to establish annual targets for the adoption of solar photovoltaic systems in homes, industries, commercial businesses, public authorities and rural areas, prioritizing the service goods of the photovoltaic solar production. Revise all the incentives listed above, with the objective of reducing investment costs by enabling solar energy to reach the most remote places in the country.

8 Methodology for calculating energy production and economic evaluation

The PVF- CHART program (which designs and analyzes photovoltaic systems using methods developed at University of Wisconsin) will be used, in this work, to perform production calculations to define the necessary subsidies for the implementation of solar plants in large cities in the form of distributed generation, comparing them with the costs of installation, operation and transmission of the centralized hydroelectric generation in Brazil.

9 Final conclusions

This work will encourage the country to receive the solar source without resistance within the Brazilian energy matrix. Brazil is willing to explore this energy.

10 Acknowledgments

The author thanks Prof Costa Filho, MAF for the academic support.

References

[1] ANEEL. *Atlas of Electric Energy of Brazil. Brasilia.* 2008.

[2] R. M. da Silva. Legislative consultancy studies and research center - solar energy in brazil: from incentives to challenges. 2015.

[3] M.A. F. N. Santos, B. C. C. Filho. Public policies to encourage photovoltaic power generation. 2017.

A MATHEMATICAL ECOLOGY MODEL FOR PEST CONTROL BASED ON POPULATION DYNAMICS

Author: Daniela Ribeiro Monteiro[1] *danielarmonteiro@gmail.com*
Advisor(s): J. F. Meyer,
Carlos A. de Moura[1]

[1] Rio de Janeiro State University

Dec 04, 2020

PPG-EM Seminars: season **2020**
http://www.ppgem.uerj.br

Keywords: Pest Control, Lotka-Volterra, Ecology, EMBRAPA.

1 Introduction

The present thesis proposes an alternative approach for the mathematical simulation of a worrisome scenario in ecology: the control of pests [1] harmful to a given soybean crop in a specific geographic region. The applied tool is the use of mathematical control, in order to couple tools of discrete mathematics to the analysis and solution of initial value problems in differential equations, namely, the so-called Lotka-Volterra [2][3] population dynamics equations with competition. These equations, which model interaction behavior among species present in a medium (such as population dynamics in a predator-prey relationship), have, with the parameters initially used, a breakeven with higher levels of pest than desired in the agricultural context under study, resulting in the need to make use of optimal control theory.

2 Objective

Ecology is the science that researches the interactions between organisms and their environment, that is, it is the scientific study of the distribution – abundance or scarcity – of living beings and the interactions that determine this distribution. The interactions can be between living beings and / or with the environment. Mathematical ecology proposes the use of mathematical models to analyze, evaluate, predict ecological phenomena. Modeling mathematically a real phenomenon consists in establishing a correspondence between quantities, actions, beings, events in a given context of the universe and mathematical variables subject to certain relations.

This work presents a real problem in agriculture: pest control, specifically, in the soy crops, the main product of Brazilian agriculture [4]. To perform this control, we used the Lotka-Volterra equations with competition in conjunction with a non-linear dispersion / diffusion-advection / transport EDP [5] whose reaction term depends on the state variable that represents the fungus. The aim is to reach optimal values from the equations that model the interspecific interaction.

Figure 1: Soy caterpillar.

Soy crops are attacked by caterpillars that eat up their leaves. Embrapa has determined that up to 20 small caterpillars or 7 large ones per meter are controllable values, or else when the defoliation reaches 30%, before flowering, or 15%, as soon as the first flowers appear. Whenever this threshold is attained, a control method is needed so that no serious economic damage is made to the crop. For this control, pesticides or biological controls are employed, such as: viruses, fungi and bacteria.

3 Mathematical Model

Let P_1 and P_2 be two interacting populations. A mathematical model which describes their relationship, where $P_1 = P_1(x, y, t)$, $P_2 = P_2(x, y, t)$, $t \in (0, T]$, $(x, y) \in \Omega \subset \mathbb{R}^2$ is given by the system:

$$\frac{\partial P_1}{\partial t} = div(\alpha_1 \nabla P_1) - div(\mathbb{V} P_1) - \sigma_1(x, y, t) P_1 - c_1 P_1 P_2 + F_1$$

$$\frac{\partial P_2}{\partial t} = div(\alpha_2 \nabla P_2) - div(\mathbb{W} P_2) - \sigma_2(x, y, t) P_2 + c_2 P_1 P_2 + F_2$$

The domain Ω represents the considered medium and, for $i = 1, 2$,

$P_i = P_i(x, y, t)$ population or population densities
$\alpha_i = \alpha_i(x, y, t)$ the population diffusion or dispersion coefficients

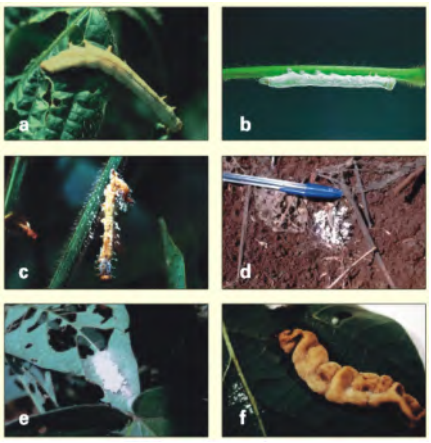

Figure 2: (a) – soy caterpillar infected by virus; (b) – soy caterpillar infected by *Nomuraea rileyi*; (c) – *Plusiinae* infected by *Zoophtora radicans*; (d) – soy caterpillar infected by *Paecilomyces tenuipes*; (e) – *Plusiinae* infected by *P. tenuipes*; (f) – *Plusiinae* infected by *Pandora gammae*.

$\sigma_i = \sigma_i(x, y, t)$ the hostility rates of species in the medium Ω during the period $[0, T]$
$\mathbb{V}$ e $\mathbb{W}$ the vectors of the field of population migration or advection speeds
c_i is the rate of interspecific ratio
F_i is a population dynamics of the species, in the medium Ω during the period $[0, T]$

For the predator-prey model studied, the two populations P_1 and P_2 that interact will be studied with some adaptation.

The proposed model is described as follows:

$$\begin{array}{c} \frac{dF}{dt} = \lambda_F F\left(1 - \frac{F}{K+L}\right) + \beta_{FL} FL \\ \frac{\partial L}{\partial t} -_L \triangle L + \mathbb{V} \cdot \bigtriangledown L = \lambda_L \left(1 - \frac{L}{M}\right) - \beta_{LF} LF \ , \end{array} \tag{1}$$

where $\mathbb{V} =< u, v >$, with initial conditions:

$F(0) = F_0$.
$L(x, y, 0)|_{\partial\Omega} = L_0(x, y)_{\partial\Omega}$.

Equation [1] will be discretized in space using the centered Finite Difference Method. In time, the Crank Nicolson Method will be chosen. Equation [1] will then look like:

$$\begin{array}{c} \frac{dF}{dt} = \lambda_F F\left(1 - \frac{F}{K+L}\right) + \beta_{FL} FL \\ \frac{\partial L}{\partial t} = \alpha_L \left(\frac{\partial^2 L}{\partial x^2} + \frac{\partial^2 L}{\partial y^2}\right) - u\frac{\partial L}{\partial x} - v\frac{\partial L}{\partial y} + \lambda_L L\left(1 - \frac{L}{M}\right) - \beta_{LF} LF \end{array}$$

Denote $F(x_i, y_i, t_n) \simeq F_i^{(n)}$ and use the finite difference centered method, in order to reach:

$$\frac{F_i^{(n+1)} - F_i^{(n)}}{\Delta t} = \lambda_F \frac{F_i^{(n)} + F_i^{(n+1)}}{2}\left(1 - \frac{F_i^{(n)} + F_i^{(n+1)}}{2K + L_i^{(n)} + L_i^{(n+1)}}\right)$$

4 Conclusions

The proposed model was programmed in Octave, using the finite difference space-centered method coupled to the Crank-Nicolson scheme for time discretization. It was possible to see the fungus dispersion in the crop and its action as a biological control, leading to a decrease in the number of caterpillars per meter and their dissipation in the environment.

5 Acknowledgments

The author would like to especially thank this research advisor, Carlos Antônio de Moura, its co-advisor, João Frederico da Costa Azevedo Meyer, from Unicamp, and CAPES for the financial support.

References

[1] ZAMBOLIM, Laercio; PICANÇO, Marcelo Coutinho (Ed.). *Controle Biologico – Pragas e Doenças: Exemplos Praticos*. Viçosa: Universidade Federal de Viçosa, 2003, 310 p.

[2] VOLTERRA. V.:*Fluctuations in the abundance of a species considered mathematically, 1926*.

[3] LOTKA, A.J.: *Elements of Physical Biology, 1925*. Williams & Wilkins Company, Baltimore.

[4] EMBRAPA Soja. Available in: *https://www.embrapa.br/soja/cultivos/soja1/dados-economicos*. Access: 13 dec. 2020.

[5] BOYCE, W. E.; DIPRIMA, R.C.: *Equações Diferenciais Elementares e Problemas de Valores de Contorno, 1998*. LTC, Rio de Janeiro, 6 ed.

PPG-EM
Programa de Pós-graduação em Engenharia Mecânica

STOCHASTIC COMPUTATIONAL SIMULATIONS OF FILOPODIAL GROWTH UNDER INFLUENCE OF REGULATORY PROTEINS

Author: Thiago Franco Leal[1] *thiagofranco@ime.uerj.br*
Advisors: Carlos Antônio de Moura[1] ; Maurício Vieira Kritz[2] ; Andreas Prokop[3]
[1] Rio de Janeiro State University ; [2] National Laboratory of Scientific Computation ; [3] University of Manchester

PPG-EM Seminars: season **2020**
http://www.ppgem.uerj.br
December 2, 2020

Keywords: Cytoskeleton, Filopodia, Computational model, Transport phenomena

1 Introduction

Actin is the most abundant protein in eukaryotic cells. Actin monomers (G-actin) are building blocks to form the cytoskeleton, a network of filamentous polymers (F-actin) that sustains the cell membrane. F-actin can be arranged into parallel bundles to mediate the formation of filopodia, which are finger-like organelles to sense the environment [5]. See Figure 1.

To understand actin transport in filopodia (Section 2), this work presents the premises for a stochastic model of filopodial dynamics (Section 3). Unlike previous attempts [6], this model drives molecules displacement by adding the advective effect of cytoplasmic flow to diffusion. Then, the model is used to observe how filopodia evolves when regulated by specific regulatory proteins (Section 4).

2 Biological context: Filopodia

In filopodia, F-actin bundle undergoes constant backflow driven by polymerization at the filopodial tip and concomitant disassembly at the base. This makes filopodia elongate, retract, or present a steady-state equilibrium. To elongate, G-actins must travel through the entire length of the filopodium to supply polymerization and maintain F-actin backflow.

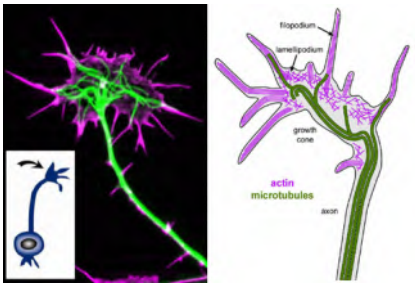

Figure 1: Filopodia on a neuronal growth cone. Image kindly provided by A. Prokop.

The simple organization of filopodia offers the advantage of being regulated by few specialized molecules, namely actin binding proteins (ABP's). Of particular interest are profilin (which performs G-actin sequestration to favor its transport) and Ena/VASP (that regulates F-actin tips enhancing G-actin polymerization due to a high attraction to actin-profilin complexes) [1, 2].

3 Two-phase model formulation

In [3], we show that diffusion does not deliver enough G-actin to sustain the backflow. Diffusion seems to be a proper first model for G-actin motion in short protrusions ($\sim 0.5\ \mu$m) [4], but needs to be combined with other phenomena to explain lengths observed *in vivo*. Therefore, the advective effect of the cytoplasm flow is an additional mechanism proposed here.

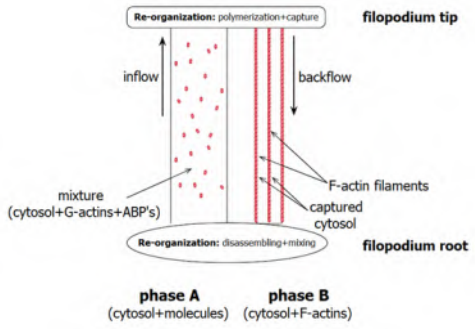

Figure 2: Two-phase model scheme. Image kindly provided by M.V. Kritz.

Assuming a sufficiently rigid membrane, F-actin constant backflow extracts volume from the very tip generating a negative pressure. This triggers a compensatory inflow of cytoplasm. The outflow volume is straightly related to the number of filaments in the bundle N, the spacing s between them, and filopodial length L itself. These parameters impact the mass balance within filopodia.

Also, the polymerization rearrange the fluid into two phases: the inflow cytosol with molecules suspended outflowing as filaments with cytosol trapped between then, as illustrated in Figure 2. From this statement, we can compute $V_{out} = f(N,L,s)$ since $V_{in} = V_{out}$, being V_{in} and V_{out} the amount of inflow and outflow volumes, respectively.

4 ABP's influence on filopodial dynamics: results and discussion

In the following tests, we investigate profilin and Ena/VASP influences on filopodial growth by including ("on") or eliminating ("off") them of the system. The red line shows the G-actin critical concentration, on which filopodial growth decreases. This explains the oscilation of L and the stochastic approach.

- Ena/VASP = "off", Profilin = "off": without regulators, the effect of adding advection to molecules displacement can be seen already, as filopodium reachs 1.7 μm. See Figure 3.

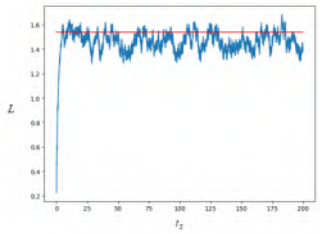

Figure 3: Filopodial length without biological regulation.

- Ena/VASP = "on", Profilin = "on": both regulators taking place; filopodial elongation is improved, varying between values higher than those when there were no ABP's in the system. See Figure 4.

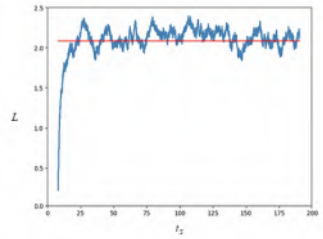

Figure 4: Filopodial length with biological regulation.

- Ena/VASP = "off", Profilin = "on": G-actin sequestration decreases polymerization rate, which shortens filopodial length. See Figure 5 for different tested amount of profilin.

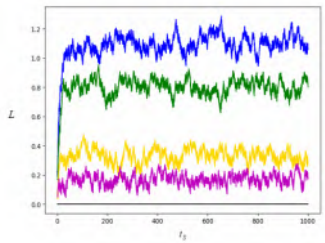

Figure 5: Influence of profilin. In blue, 0% (all G-actins are free); in green, 20%; in yellow, 50%; and in magenta, 60%.

- Ena/VASP = "on", Profilin = "off": as Ena/VASP binds F-actin tips, the polymerization rate decreases drastically, since no profilin are present to interact with Ena/VASP. But when there is a number of free G-actins, polymerization can still occurs. See Figures 6 to observe scenarios with different amount of profilin.

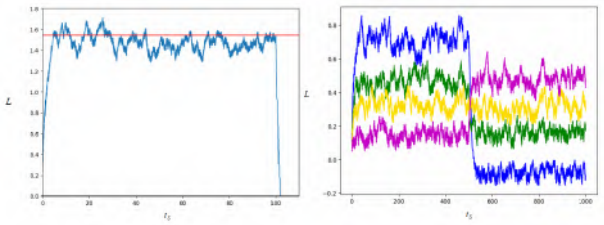

Figure 6: Ena/VASP regulating tip. In the left, there is no profilin. In the right, different amounts of profilin (in blue, 0% (all G-actins are free); in green, 20%; in yellow, 50%; and in magenta, 60%).

5 Conclusions

The computational model formulated allows us to inquire the effects of the presence/absence of any combination of ABP's aiming to observe how the filopodial length behaves accordingly. From these results:

- profilin and Ena/VASP greatly enhances G-actin polymerization;
- the absence of any of these regulators in the system will decrease filopodial growth;
- advection-diffusion coupling increases filopodial growth efficiency by supporting F-actin bundle backflow.

These above concepts and results comprise a brief description of an application present in the author's thesis. Some of these results have already been discussed in the literature and they serve to validate the proposed model. In the thesis, the model is able to develop filopodia with lengths of almost 20 times higher than those in previous efforts that used just diffusion as transport phenomena.

References

[1] J.E. Bear and F.B. Gertler. Ena/vasp: towards resolving a pointed controversy at the barbed end. *J. Cell. Sci.*, 122, 2009.

[2] A. Birbach. Profilin, a multi-modal regulator of neuronal plasticity. *Bioessays*, 30, 2008.

[3] C.A. de Moura, M.V. Kritz, T.F. Leal, and A. Prokop. Mathematical-computational simulation of cytoskeletal dynamics. *Springer-Verlag*, 2016.

[4] A. Mogilner and R. Rubinstein. The physics of filopodial protrusion. *Biophys. J.*, 89, 2005.

[5] B. Alberts et al. *Molecular Biology of the Cell.* New York: Garland Science, 2002.

[6] J.A. Ditlev et al. There is more than one way to model an elephant: experiment-driven modeling of the actin cytoskeleton. *Biophys. J.*, 104, 2013.

IMPROVED ANISOTROPIC TRANSPORT THROUGH POLYMER LAYER AND POROUS ARTERIAL WALL WITH BINDING IN DRUG-ELUTING STENTS

Author: Fabiane Frazzoli[1] *frazzoli.fabi@gmail.com*
Advisor(s): Norberto Mangiavacchi, Rachel Lucena[1]
[1] Rio de Janeiro State University

PPG-EM Seminars: season **2020**
http://www.ppgem.uerj.br
December 16, 2020

Keywords: Drug-eluting stents, Darcy's law, anisotropic diffusion, finite element method

1 Introduction

One of the revolutions in percutaneous coronary intervention (PCI) was the development of drug-eluting stents (DES). It consists of a small coated pipe mesh with antiproliferative drugs (Sirolimus) that is implanted in the arterial wall, treating the stenosis, removing the obstruction and allowing the blood flow. The efficiency of the drug is influenced by the anisotropic transport of Sirolimus in the arterial all and for dissolution and specific binding of the polymeric layer. In this work we intend to evaluate impact of anisotropic diffusion tensor and the laplacian approach in comparison with the work presented by Lucena *et al.* [2], where the principal directions were obtained through an orthogonal tensor.

2 Methodology

We propose in this work a computational model of dissolution, transport and binding of sirolimus in an axisymmetric domain represented by the polymer coating layer and the arterial wall as proposed by McGinty and Pontrelli[3] and Bozsak *et al.*[1]. An example of an unstructured triangular mesh employed in the simulations is shown in Figure 1.

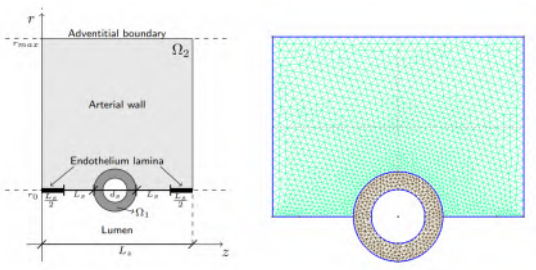

Figure 1: 2D axisymmetric geometry model (left) and the computational unstructured triangular mesh employed in the simulations (right).

The arterial wall and the polymer layer are considered as porous media, and flow within these layers is assumed to be incompressbile and governed by Darcy's law $\mathbf{u} = -\kappa_i \nabla p$, thus $\nabla \cdot (-\kappa_i \nabla p) = 0$, where $\mathbf{u} = (u, v)$ is the velocity field, p is the pressure in the arterial wall, $\kappa_i = P_{Di}/\mu$, P_{Di} is the Darcy permeability of the media and μ is the fluid viscosity.

The drug dynamics in the coating are governed by concentrations equations:

$$\frac{\partial b_0}{\partial t} = -\beta_0 b_0^{2/3}(S_0 - c_0) \quad (1)$$

$$\frac{Dc_0}{Dt} = \nabla \cdot (\mathcal{D}_0 \nabla c_0) + \beta_0 b_0^{2/3}(S_0 - c_0), \quad (2)$$

where the operator D/Dt is the material derivative, b_0 and c_0 are solid and dissolved concentrations. $\mathcal{D}_0$ is the effective scalar diffusion coefficient of the solute, β_0 the dissolution rate and S_0 is the solubility limit.

Drug elution in the arterial wall is governed by the convection-diffusion-reaction equations:

$$\frac{Dc_1}{Dt} = \nabla \cdot (\mathcal{D}_1 \nabla c_1) - k_1^f c_1 (b_1^{max} - b_1) + k_1^r b_1 - k_2^f c_1 (b_2^{max} - b_2) + k_2^r b_2 \quad (3)$$

$$\frac{\partial b_1}{\partial t} = k_1^f c_1 (b_1^{max} - b_1) - k_1^r b_1 \quad (4)$$

$$\frac{\partial b_2}{\partial t} = k_2^f c_1 (b_2^{max} - b_2) - k_2^r b_2, \quad (5)$$

where c_1 is the concentration of a drug transported in the arterial wall b_1 and b_2 denote non-specifically and specifically bound drug, respectively, k_i^f, k_i^r, b_i^{max} are constant parameters related to the binding kinetics, and $\mathcal{D}_1$ is diffusion coefficient gives by the an anisotropic tensor.

The permeability in the polymer coating, P_{D0}, is considered to be very small, but finite. The endothelium lamina, where present, is modeled as a no-flow boundary. The boundary conditions on drug in the denuded endothelium is $c_1 = 0$, between polymer and blood, i.e., on interface Γ_1 is $c_0 = 0$, (see Fig. 2). We assume periodic conditions at the side boundaries. The mass flux is established across the interface and the drug starts to be transferred to the adjacent release medium.

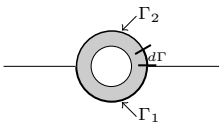

Figure 2: Sketch of interface polymer-lumen and polymer-arterial wall [2].

A Matlab code was developed to solve the governing equations in 2D axisymmetric coordinates applying an unstructured triangular mesh and using linear base functions and the Galerkin Finite Element Method. The convective terms are discretized using a semi-Lagrangian approach. The Darcy flow is considered to be steady, and driven by the average pressure difference between the lumen and the adventitial boundary. A semi-implicit fractional step method is employed for the convection-diffusion-reaction equations.

3 Results

The objective of this study is to evaluate the effect of the anisotropic diffusion tensor using the laplacian approach for evaluate the principal directions compared to the results obtained by Lucena *et al.*[2], where the orthogonal tensor was adopted. Based on the results obtained we plot the difference between the field concentration for the cases, as shown in Fig. 3. A greater effect can be seen, in absolute values, between the two media addressed in the upper region stent, in contact with the arterial wall.

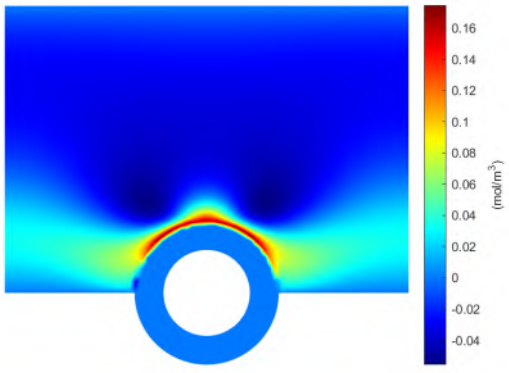

Figure 3: Two dimensional concentration differences between the anisotropic and the orthotropic mediums at $t = 15$ days.

Proceeding with the quantification of the results, Fig. 4 show the concentration at an horizontal line chosen in the arterial wall above the stent. The red curve refers to the orthotropic tensor and blue curve to anisotropic note that the concentration distribution is higher for the case orthotropic. The difference between the curves was 10^{-4}.

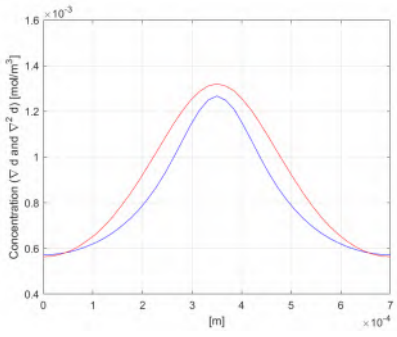

Figure 4: Two dimensional concentration differences between the anisotropic and the orthotropic mediums at $t = 15$ days.

The total amount of mass in moles of the drug, transferred to the arterial wall and the lumen obtained with both models (Anisotropic vs. Orthotropic) is show in Fig. 5. Where we see a small difference of the order of 10^{-3}.

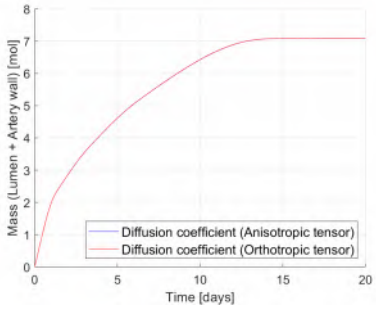

Figure 5: Mass (Anisotropic x Orthotropic tensor) and Difference of mass.

4 Conclusions

From the results obtained, we conclude that the difference between the two tensors addressed was greater upper part of the stent in contact with the arterial wall. Thus, the anisotropic tensor induced by the directions principal values calculated by the Laplacian method has an effect on the model and consequently on the result more realistic of the problem.

References

[1] Franz Bozsak, Jean Marc Chomaz, and Abdul I. Barakat. Modeling the transport of drugs eluted from stents: Physical phenomena driving drug distribution in the arterial wall. *Biomechanics and Modeling in Mechanobiology*, 13(2):327–347, 2014. ISSN 16177940. doi: 10.1007/s10237-013-0546-4.

[2] R.M. Lucena, N. Mangiavacchi, J. Pontes, G. Anjos, and S. McGinty. On the transport through polymer layer and porous arterial wall in drug-eluting stents. *Journal of the Brazilian Society of Mechanical Sciences and Engineering*, 40(572), 2018.

[3] Sean McGinty and Giuseppe Pontrelli. On the role of specific drug binding in modelling arterial eluting stents. *Journal of Mathematical Chemistry*, 54(4):967–976, 2016. ISSN 15728897. doi: 10.1007/s10910-016-0618-7.